Applied Catalysis B: Environmental 172–173 (2015) 145–153

Contents lists available at ScienceDirect

Applied Catalysis B: Environmental

journal homepage: www.elsevier.com/locate/apcatb

Evaluation of Co, La, and Mn promoted Rh catalysts for autothermal reforming of commercial diesel: Aging and characterization

Moa Z. Granlund[a,*], Kjell Jansson[b], Marita Nilsson[c], Jazaer Dawody[d], Lars J. Pettersson[a,e]

[a] KTH Royal Institute of Technology, Department of Chemical Engineering and Technology, SE-100 44 Stockholm, Sweden
[b] Stockholm University, Arrhenius Laboratory, Department of Materials and Environmental Chemistry, SE-106 91 Stockholm, Sweden
[c] Scania CV AB, Materials Technology, Engine Performance and Emissions, SE-151 87 Södertälje, Sweden
[d] Volvo Group Trucks Technology, Advanced Technology and Research, Energy Efficiency and Environment, SE-412 88 Göteborg, Sweden
[e] Stellenbosch Institute for Advanced Study (STIAS), Wallenberg Research Centre at Stellenbosch University, Marais Street, 7600 Stellenbosch, South Africa

ARTICLE INFO

Article history:
Received 6 November 2014
Received in revised form 11 February 2015
Accepted 15 February 2015
Available online 18 February 2015

Keywords:
Autothermal reforming
Characterization
Diesel
Deactivation
Morphology

ABSTRACT

In this study, three bimetallic catalysts are evaluated for autothermal reforming (ATR) of fuels (1 wt.% Rh and 6 wt.% X (X = Co, La or Mn) supported on high-surface area CeO_2–ZrO_2). The catalysts are aged for approximately 35 h and carefully characterized both as fresh and aged materials. The objective is to illuminate the changes in material properties after time on stream as well as the differences among the materials. The changes in material properties are evaluated by H_2-TPR, BET surface area analysis, TEM, SEM, and STEM. The material's tendency to coke is investigated by TPO analysis.

The three materials exhibit promising initial activity. However, the Co-promoted sample decreases sharply in activity after 25 h of operation. Meanwhile, the other two materials display a more stable activity throughout the evaluated time. The deactivation of the Co-promoted material could be linked to the high amount of coke deposited during operation. Based on the results from the activity evaluation and characterization, the material promoted with lanthanum displays the most promising results. The addition of lanthanum resulted in a catalyst that was both stable and had high activity, even though a low rhodium loading is used. The material also shows superior thermal resistance compared to the other two materials. In addition, the tendency to coke is significantly lower compered to the other materials, which is especially beneficial when dealing with ATR of complex fuels.

1. Introduction

There is an urgent need to reduce the fuel consumption and the emission levels from the transport sector, due to both limited resources of fossil fuels and the issues connected to global warming. Hydrogen has long been pointed out as a promising near-future replacement to fossil fuels in both stationary and mobile applications. For smaller cars, hydrogen is a viable fuel for propulsion, but for larger vehicles such as heavy-duty diesel vehicles (HDDVs) this is not an option due to the limited power output of the system. Instead, hydrogen can be used in other applications in HDDV's: (i) as fuel to a fuel cell, generating electricity in an auxiliary power unit (FC APU) [1–3], (ii) as additive to hydrocarbon-assisted lean NO_x reduction catalyst (HC-LNC) [4,5], (iii) heating of the exhausts to decrease the start-up time for the aftertreatment catalysts, and (iv) supplementary fuel for auxiliary equipment.

Among the various applications for hydrogen onboard, the usage of an APU would have the greatest positive influence on both the emission levels and fuel consumption. The produced electricity of the system would be used instead of idling the engine during rests. This would have a significant influence on the total emission since idling emission stands for approximately 10% of the total emissions [6]. Usage of an FC APU as power generator during standstills would also mean less wear of the engine and prolong its lifetime [7,8]. An FC APU consists of a fuel cell, a fuel reformer, and a cleanup system for the reformate. The fuel reformer provides the fuel cell with hydrogen, which in turn produces the electricity. The production of hydrogen via fuel reforming is a versatile hydrogen source since the problems connected with storage and availability of hydrogen are eliminated and the fuel is easily available in an already existing and well-developed infrastructure [9]. It is also an advantage to use the propellant as hydrogen source to avoid having two different fuel tanks on the vehicle.

However, there are several aspects that need to be considered in fuel reforming and many of them are connected to the catalytic material itself and the reforming process. The reforming process

* Corresponding author. Tel.: +46 730460300.
E-mail address: moazg@kth.se (M.Z. Granlund).

http://dx.doi.org/10.1016/j.apcatb.2015.02.018
0926-3373/

often used in vehicle applications is autothermal reforming (ATR). The main reasons are the fast thermal response of the process together with the high H_2 yield. Additionally, ATR requires no external heating. The fact that both oxygen and steam is present in the reactant mixture makes the process suitable for reforming of commercial fuels. The oxygen contributes to a fast pre-reforming of the fuel, making it easier to steam reform. The steam together with the oxygen also increases the gasification rate of deposited coke and thereby limits the total coke amount compared to steam reforming and partial oxidation [10]. For the catalyst to withstand the harsh operating conditions, it is often loaded with of one or more of the platinum group metals (PGM), where Rh is the most commonly used metal. However, the PGM metals are expensive and the resources are limited. Hence, there is a wish to decrease the rhodium content without compromising the catalytic activity and stability.

This article is the second of two papers evaluating cobalt's, lanthanum's, and manganese's potential as additive in diesel ATR catalysts. The aim is to decrease the rhodium content by 2/3, from 3 wt.% down to 1 wt.%, without sacrificing the catalytic activity. The evaluated catalysts are 1 wt.% Rh/6 wt.% X (X = Co, La or Mn) and are compared with a reference catalyst containing 3 wt.% Rh. All four catalysts are supported on high-surface area CeO_2–ZrO_2. Motivation to why these three transition metals were chosen as candidates can be found in the first article [11]. The first article covers catalytic activity and basic characterization (X-ray diffraction (XRD), surface area measurements, and H_2 temperature-programmed reduction (TPR) of fresh materials). This article, on the other hand, includes aging of the catalytic material and further characterization of both fresh and aged materials (temperature-programmed oxidation (TPO), transmission electron microscopy (TEM), scanning electron microscopy (SEM), scanning transmission electron microscopy (STEM) and additional H_2-TPR of aged materials).

2. Experimental

2.1. ATR aging experiments

The ATR aging experiments were performed in a horizontally mounted high-temperature steel monolith reactor (Sandvik 253 MA, $\emptyset_{inner}$ = 24.3 mm). The evaluation was performed with commercial Swedish Environmental Class 1 diesel (MK1). The product gases were analyzed with an FTIR instrument (MKS Instruments, Multigas™ 230 *HS*), a mass spectrometer (V & F Instruments Inc., H-sense) and a gas chromatograph (Varian CP-3800). A detailed description of the fuel reformer setup can be found elsewhere together with physical and chemical properties of MK1 [11]. During the ATR experiments the reactant ratios were: $H_2O/C \sim 2.5$ and $O_2/C \sim 0.45$. The reactant flow was diluted in N_2 to achieve a gas hourly space velocity of $\sim$50,000 h^{-1}.

Prior to the ATR experiments, the catalysts were treated in flowing N_2 at 950 °C for 30 min. The experimental sequence consisted of a stepwise increase of temperature (50 °C/step) from 750 °C to 950 °C, which was repeated in total 7 times, resulting in a total time on stream of approximately 35 h. At each temperature step measurements were acquired for at least 45 min to ensure steady-state conditions. Product analysis and calculations are described in detailed in Ref. [11]. After each experimental sequence the catalyst was regenerated in a mixture of steam and oxygen at elevated temperature until no CO_2 signal was detected, hence only irreversible deactivation is measured. After the 7th cycle no regeneration was performed in order to be able to measure the amount of coke deposited during the cycle.

2.2. Catalyst preparation

The catalytic materials were prepared by the incipient wetness method and coated onto honeycomb cordierite monoliths (400 cpsi, $\emptyset$ = 20 mm, l = 30 mm). The support used was a high surface area CeO_2–ZrO_2 (16.5 wt.% CeO_2, MEL Chemicals). The metal precursors used were Rh nitrate solution ($Rh(NO_3)_3$, 9.53 w/w, Sigma–Aldrich), Co nitrate ($Co(NO_3)_2{\cdot}6H_2O$, Alfa Aesar), La nitrate ($La(NO_3)_3{\cdot}6H_2O$, Alfa Aesar), and Mn nitrate ($Mn(NO_3)_2{\cdot}xH_2O$, Alfa Aesar). A detailed description of the catalyst preparation can be found elsewhere [11].

2.3. Catalyst characterization

The catalytic materials were characterized with temperature-programmed oxidation (TPO), temperature-programmed reduction (TPR), scanning electron microscopy (SEM), and transmission electron microscopy (TEM). The aged catalytic material was carefully removed from the monolith to minimize the contribution from the cordierite substrate. The results from characterization of aged material should be considered as the average change in the materials after time on stream since no consideration was taken to the material's position in the monolith due to limited amount of aged material.

TPO analysis was performed in the reactor setup after the 7th temperature ramp. The reaction was quenched by simultaneously cutting fuel, air and water flows, followed by cooling of the catalyst in flowing N_2 to ambient temperature. The TPO analysis was subsequently performed by exposing the catalyst to a gas mixture of $\sim$5 vol.% O_2 in N_2, meanwhile the temperature was ramped to 950 °C (5 °C/min) meanwhile the CO_2 was analyzed. The sample was left at 950 °C in the oxidizing atmosphere until no CO_2 could be detected.

The TPR analyses were performed in a Micromeritics Autochem 2910 apparatus. Before the measurements, the samples were completely reduced and oxidized at 950 °C to ensure complete oxidation and removal of impurities. During the analysis, the samples were exposed to 5 vol.% H_2 in He meanwhile the temperature was ramped from ambient to 950 °C (5 °C/min).

Prior to the electron microscopy investigations, the catalyst materials were applied on a perforated carbon film and supported on a standard copper grid. Three-dimensional images were obtained with SEM (Jeol 7000F) and high-resolution images were obtained with TEM (Jeol 2100F). Both electron microscopes were equipped with energy dispersive X-ray spectroscopy detectors (EDS). The element distributions were determined by spot measurements and element mapping, using accelerating voltages of 15 kV in SEM and 200 kV in TEM. The spot EDS measurements were performed with a beam size less than 10 nm.

3. Results and discussion

3.1. ATR deactivation experiments

During ATR of diesel, the catalyst is exposed to several deactivation threats, lowering the activity and eventually catalyst failure. To be able to find a suitable catalyst for ATR of diesel, it is highly important to evaluate the aging processes of the materials as well as the changes of the materials as a function of time on stream. In this study, the materials were characterized as fresh materials, after thermal treatment in air at 950 °C (thermally aged) and after $\sim$35 h on stream (chemically aged). The two most important performance parameters for an ATR catalyst are H_2 yield and fuel conversion. Since the aim of the study is to decrease the Rh loading without compromising the catalytic activity by adding a suitable

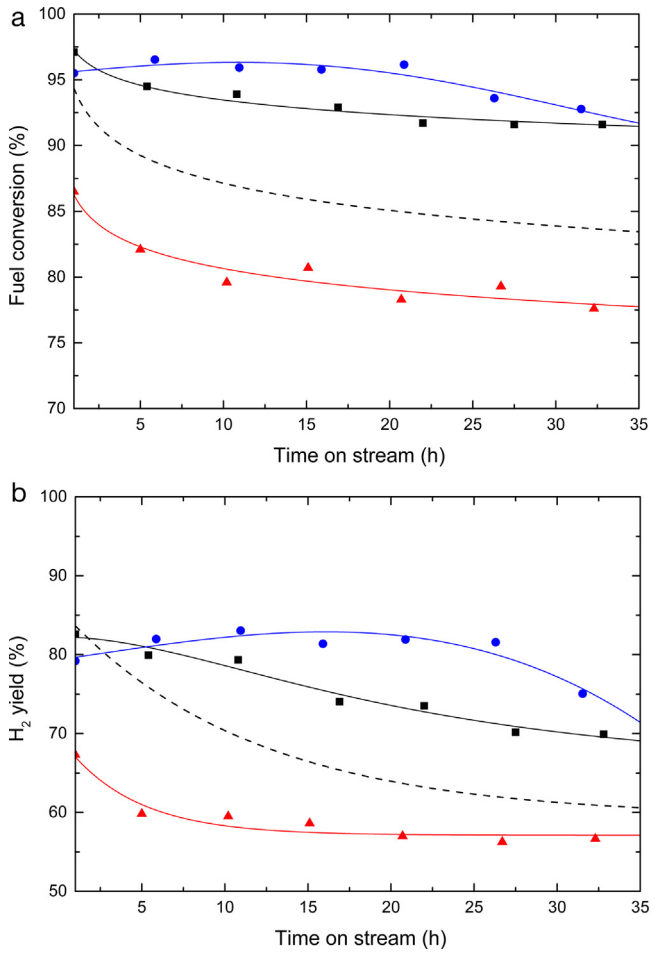

Fig. 1. Catalytic activity, (a) fuel conversion and (b) H_2 yield, at 750 °C as a function of time on stream. The catalysts are denoted as: (●) Rh(1)Co(6), (■) Rh(1)La(6), (▲) Rh(1)Mn(6) and (- - -) Rh(3) (reference material) where the numbers in parentheses are the nominal loadings (wt.%) of the current metal.

promoter, the performance of the three materials are compared with a reference material (3 wt.% Rh/CeO_2–ZrO_2).

The evaluation clearly shows that the interaction between the Rh and the promoter is of great importance for the catalytic performance and alters the product distribution significantly. The fuel conversion and the H_2 yield of the three evaluated catalysts together with the reference catalyst are displayed in Fig. 1. In the two graphs, it can be observed that the same trends can be observed for both the fuel conversion and H_2 yield. Secondly, it can be noticed that both the Co-promoted and the La-promoted catalysts exceed the activity of the reference catalyst, meanwhile the Mn-promoted material has a lower activity. The catalytic activity of this material is somewhat lower than the catalytic activity of the reference catalyst. However, the reference catalyst was evaluated with synthetic diesel (NExBTL, Neste Oil) and not MK1 at the same operating parameters. NExBTL contains very low concentrations of both aromatic compounds and sulfur and can therefore be considered less adverse for the material as well as easier to reform. As a consequence of this, the activity of the reference material is most likely slightly overestimated and the activity of the Mn-promoted material is probably comparable with the reference material. Therefore, it can be concluded that the three promoted materials exhibit comparable or enhanced catalytic activity compared to the reference material. However, this study does not focus on the differences between the evaluated materials and the reference material, but on the changes in the evaluated materials as a consequence of time on stream and the differences among them.

As can be observed in Fig. 1, the aging behaviors of the catalytic materials are considerably different. The Mn-promoted catalyst shows a fast initial decrease in both fuel conversion and H_2 yield, stabilizing after 10 h of operation. The La-promoted sample has a slower decrease in activity, where fuel conversion levels out around 15 h on stream meanwhile the H_2 yield continues to decrease slowly throughout the evaluation time.

The Co-promoted catalyst displays still another aging pattern. The material seems to go through some initial activation prior to reaching its highest activity, which is the highest activity observed of the evaluated materials. The combination of Rh and Co has previously been observed to have high catalytic activity for reforming [12,13]. The reason is believed to be cobalt's ability to suppress total oxidation and instead facilitate partial oxidation, which results in a higher H_2 yield. The increase is small but has been observed in other studies where cobalt and rhodium are combined for reforming [14]. The activity suddenly decreases sharply after 25 h on stream, not as sharp for the fuel conversion as for H_2 yield, but still considerably. What causes the different aging pattern of the materials is further investigated by comparing properties of fresh and aged materials in the following sections.

3.2. Characterization

The changes in specific surface area, average pore diameter, and crystal size of CeO_2–ZrO_2 between fresh and aged materials were reported and discussed in the previous article [11]. A summary of the results from this article is presented in Table 1. In this follow-up article, the aim is to try to explain and understand these changes in activity with further characterization of both fresh and aged materials.

As can be observed in Table 1, all the promoted samples display a significant decrease in surface area, which is attributed mainly to sintering of CeO_2, taking place readily at high temperatures and especially at reducing conditions [15,16]. Considerable sintering of CeO_2–ZrO_2 particles is visible after operation, especially for the Co and Mn-promoted materials. Despite this, the activity is not significantly affected. Therefore, it is concluded that surface area is not one of the main characteristics influencing the activity of an ATR catalyst.

3.2.1. Electron microscopy

The fresh materials were analyzed by TEM to investigate the differences between the three materials. In the analysis, it was not possible to visualize Rh particles in any of the fresh materials. The reason is probably the encapsulation of the Rh particles by the

Table 1
The changes in morphology between fresh and thermally or chemically aged materials. For thermal aging the materials were treated in air at 950 C. The chemical aging is equivalent to time on stream.

Catalytic material	Specific surface area ($SA_{950\,°C}$–$SA_{850\,°C}$) (%)	Pore diameter ($Pd_{950\,°C}$–$Pd_{850\,°C}$) (%)	Crystallite size of CeO_2–ZrO_2 ($Cs_{chemicallyaged}$–Cs_{fresh}) (% (nm))
CeO_2–ZrO_2	−23	+8	n.a.
Rh(1)Co(6)/CeO_2–ZrO_2	−22	+28	+58 (+8.3)
Rh(1)La(6)/CeO_2–ZrO_2	−15	+53	+28 (+2.0)
Rh(1)Mn(6)/CeO_2–ZrO_2	−40	+25	+157 (+15.2)

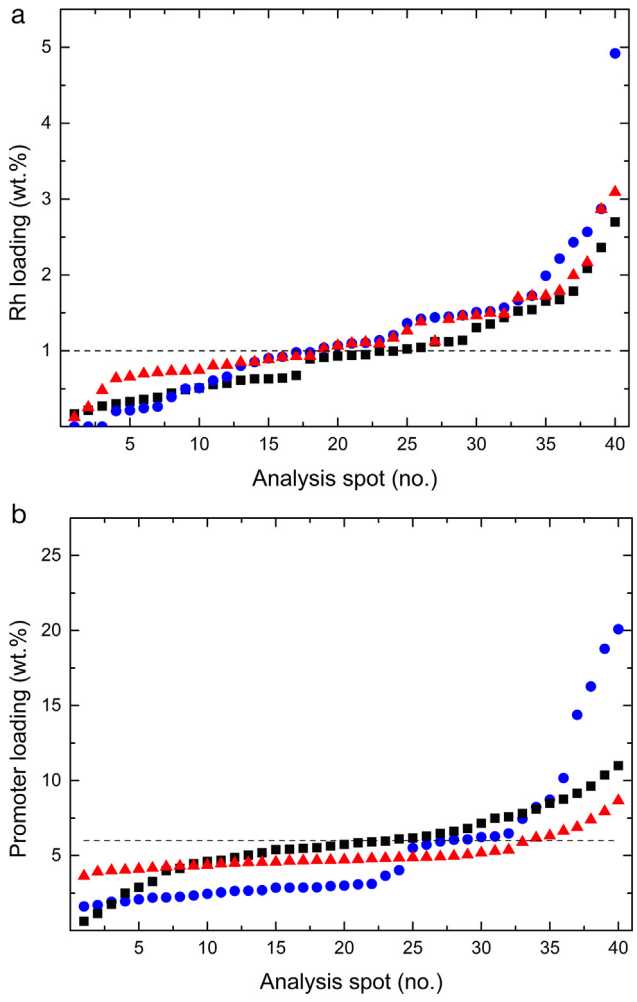

Fig. 2. Summary of spot analyses arranged according to measured (a) Rh loading and (b) promoter loading of the catalytic samples. The results of spot analyses are arranged with increasing loading of Rh and promoter, respectively. The graphs are denoted as: (●) Rh(1)Co(6), (■) Rh(1)La(6), (▲) Rh(1)Mn(6).

support, making them hard to observe by TEM [15,17]. The fresh materials were further analyzed with SEM in combination with EDS to obtain composition analysis in multiple spots to be able to visualize the dispersion of the different metals. In total, 40 EDS analyses were performed and arranged in increasing Rh and promoter loading (Fig. 2). The EDS analyses confirmed the presence of a well-dispersed Rh phase in La and Mn-promoted materials with high homogeneity and the measured Rh content corresponded well with the nominal Rh loading. Based on the nominal loading of Rh it is estimated that the crystallites are in the size range 1–2 nm. This corresponds well with previous reports stating that addition of lanthanum increases Rh dispersion [15]. It was also concluded that manganese seems to improve the dispersion of Rh as well. In addition, the EDS revealed an even dispersion of both Mn and La, and the analyzed loadings corresponded well with the nominal loading (La: 5.8 wt.% and Mn 5.1 wt.% cf. nominal loading 6 wt.%).

For the Co-promoted sample, the EDS analysis displayed a tendency for formation of larger Rh particles with clear deviation from the nominal loading of Rh. The same was observed for the dispersion of cobalt, where spots with large differences in Co loadings were detected. To further investigate the behavior of agglomeration of Rh and Co, the material was additionally investigated with EDS mapping in STEM mode. The analyses confirmed that Co was enriched into larger particles, which corresponds well with the observation with XRD in the previous article [11]. Further

Table 2
The measured total H_2 uptake for the fresh and chemically aged catalytic materials. The TPR profiles are presented in Section 3.2.2. The numbers in parentheses denotes the nominal loading (wt.%) of the current metal.

Sample	Total H_2 uptake (a.u.)	
	Fresh	Aged
Rh(1)Co(6)	8.6	10.1
Rh(1)La(6)	3.1	1.9
Rh(1)Mn(6)	4.4	2.7

STEM–EDS analysis showed a clear correlation between the enrichment of Co and Rh and it could be concluded that Rh and Co had a tendency to enrich together (Fig. 3). The presence of bimetallic particles of Rh and Co was also confirmed with TEM, where well-defined bimetallic particles were visible (Fig. 4a). This tendency for Co and Rh to form bimetallic particles has been observed earlier by others [12,13,18]. The formation of these particles is believed to be independent of the preparation method and solely a consequence of the similar chemistry between the two metals, making them completely miscible [19].

After time on stream, the materials were again analyzed by electron microscopy to evaluate the changes of the materials. In the Co-promoted material it was possible to confirm the growth of the Rh–Co bimetallic particles observed with XRD in Ref. [11] (Fig. 3b). Besides from the enlargement of the particles, the nature of the particles is changed during reaction, from being a well-defined crystalline particle in the fresh material to a spherical, less defined particle in the aged material (Fig. 4). In the Mn-promoted sample, both Mn and Rh particles were visible on the surface of the catalyst (Fig. 5b). In addition, metal particles embedded in coke were found (Fig. 9d). The Rh particles visible were 1–5 nm large and the Mn particles 5–15 nm. The particle growth of Mn was possible to confirm with XRD measurements, while the Rh particles were still not detected [11]. However, significant increase in the particle size of Rh supported on CeO_2–ZrO_2 has been observed earlier by Kim et al. [20].

Furthermore, TEM analyses enable the confirmation of the decrease in specific surface area of the La-promoted material (Table 1, Fig. 6a and b). The crystal growth of CeO_2–ZrO_2 in the material is large in percentage, almost 30%. However, the growth in real numbers is +2 nm, which is considerably less than for the other two materials. This can be derived from lanthanum's ability to stabilize the crystal phase of CeO_2–ZrO_2 [21]. The stabilization is due to the formation of an amorphous layer in between the CeO_2–ZrO_2 particles, which prohibits particle growth. It is not fully understood whether the amorphous layer consists of pure lanthanum or if ceria is dissolved into the amorphous phase as well. The layer is difficult to distinguish in the fresh material (Fig. 6a and c), but in the aged material the amorphous layer is very distinct (Fig. 6b and d). By performing STEM–EDS of the aged sample it was possible to observe a well-dispersed phase of Rh, which supports the theory that lanthanum stabilizes the Rh phase as well [15].

3.2.2. Temperature programmed reduction

The changes in reducibility between fresh and aged materials were analyzed with TPR (Fig. 7). The total H_2 uptake was calculated by integrating the area under the TPR profiles (Table 2). A detailed discussion on how the promoters affect the reducibility of CeO_2–ZrO_2 is found in Ref. [11]. The coke residues observed by TEM in aged Co and Mn-promoted materials are assumed to not interfere with the TPR analyses.

From Fig. 7 and Table 2, it is clear that the total amount of H_2 uptake and the reducibility of the catalytic materials are changing with time on stream. For the Co-promoted sample an increased H_2 uptake can be noticed after time on stream, meanwhile for the other

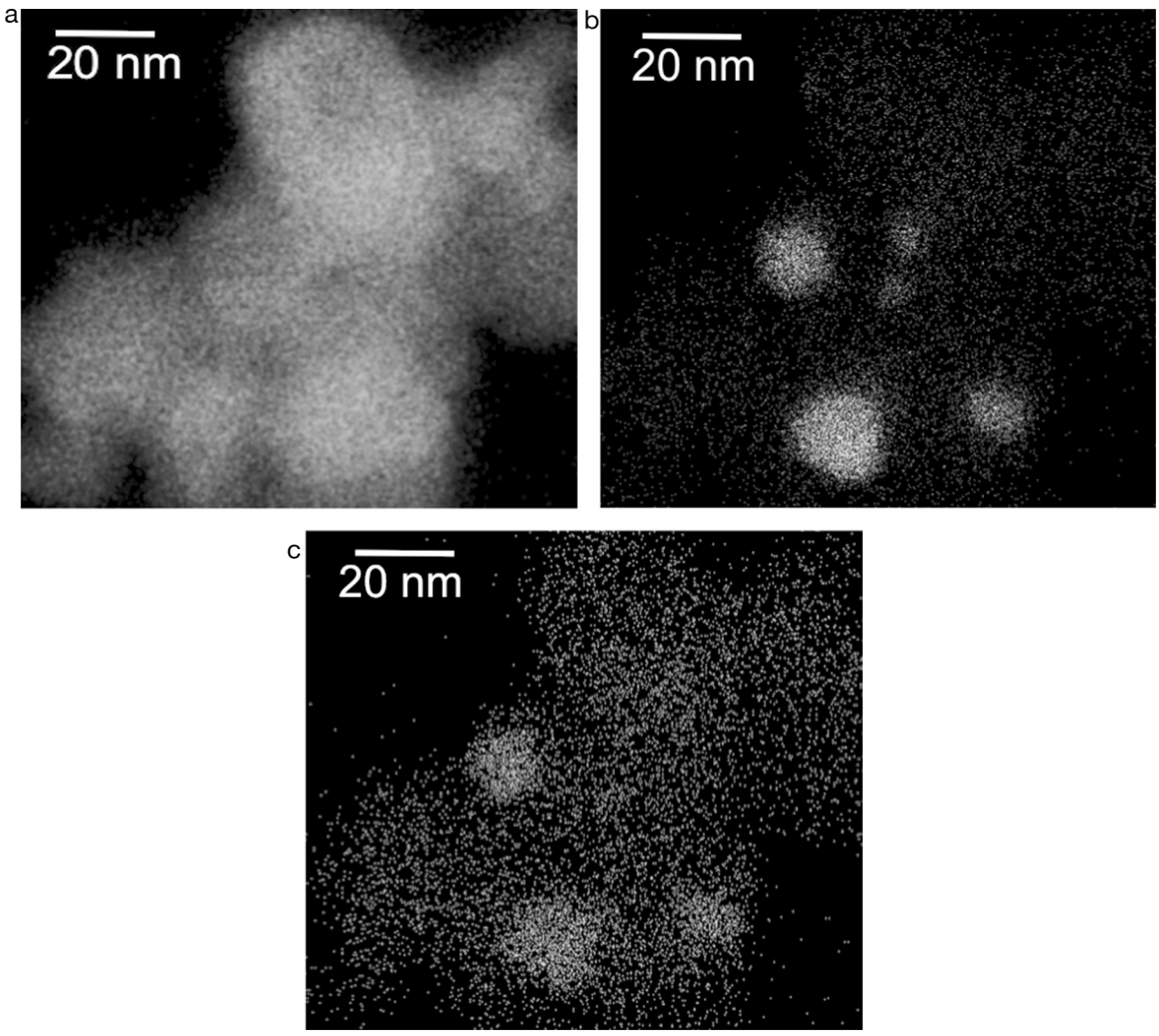

Fig. 3. Element distribution in the chemically aged Co-promoted catalyst; shown by STEM–EDS maps of the chemically aged Co-promoted sample. Distribution of (a) Zr, (b) Co and (c) Rh.

two materials the H_2 uptake has decreased approximately 40%. The materials are also reduced at lower temperature compared to the fresh samples. A combination of decreased H_2 uptake and temperature shift can be attributed to sintering of particles [15], which is in line with what was observed with the electron microscopy. The temperature shift for the La-promoted sample is small and corresponds to the observations with electron microscopy where sintering of particles was negligible. The temperature shift for the Mn-promoted sample is more than 50 °C, meaning a higher growth of metal particles, which was observed by TEM.

The TPR profiles of the Co-promoted material change considerably between the fresh and the aged materials. The profile of the fresh material displays two overlapping peaks, one at 350 °C and one at 450 °C. The two peaks are due to the fact that Co_3O_4 is a mixed oxide, consisting of CoO and Co_2O_3. Additionally, the addition of Rh strongly increases the reducibility of cobalt and increases the H_2 uptake [11,18]. In the aged sample an additional peak around 250 °C is visible, indicating the formation of new reducible species during operation. This peak appears in the temperature range where reduction of larger Rh particles is expected [22,23]. Therefore, it is believed that larger Rh particles are formed during operation from the well-dispersed Rh particles observed with STEM–EDS (Fig. 4). It has not been possible to confirm the presence of pure Rh particles by TEM. This is probably caused by the same reason to why it was not possible to visualize Rh in the fresh samples. Additionally, the TPR profile is shifted down 50 °C in temperature, which is likely to be caused by the sintering of the particles visible by both XRD and TEM. The oxidation number of Rh could explain the increase in H_2 uptake for the aged sample of Co-promoted material. When it is present as pure Rh the oxidation number is +4 meanwhile when present in in bimetallic particle together with Co the oxidation number is +3.

3.2.3. *Coke formation and coke properties*

Coking is one of the main deactivation threats for an ATR catalyst. The coking behavior is complex due to the many factors involved. First of all, there are numerous routes for coke formation, especially when using complex fuels due to the content of high-molecular weight hydrocarbons, aromatics and polyaromatics. Additionally, the formed coke can be gasified from the surface by species presence in the reformate (H_2O, H_2 and CO_2), showing the complexity of coking in an ATR reactor. To evaluate the tendency of the three evaluated materials to form coke, TPO analyses were performed after the 7th experimental cycle (Fig. 8). The total amount of coke deposited during this cycle, summarized in Table 3, was calculated by integrating the area under the CO_2 signal plotted against time until no CO_2 could be detected. After the TPO analysis, the samples were examined with TEM.

The three materials exhibit significantly different coking behaviors and the total amount of coke deposited varies. The La-promoted

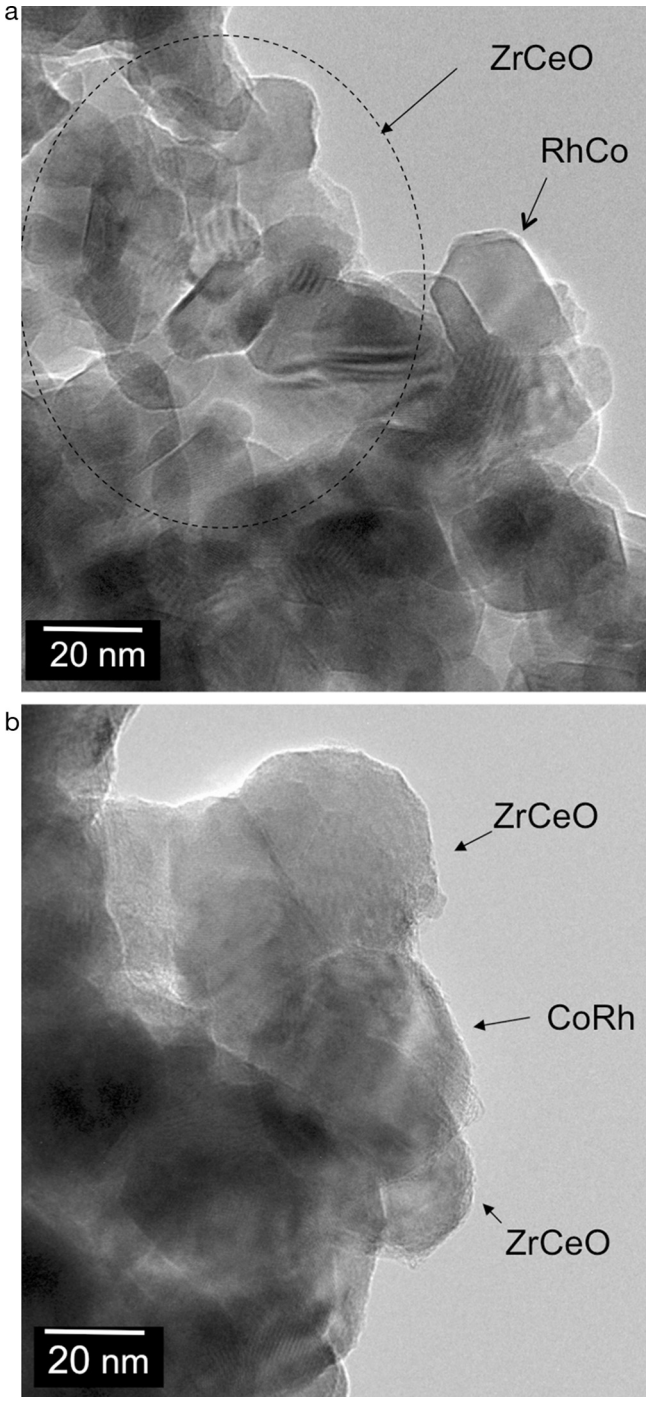

Fig. 4. TEM picture of the Mn-promoted sample ((a and c) fresh sample, (b and d) aged sample).

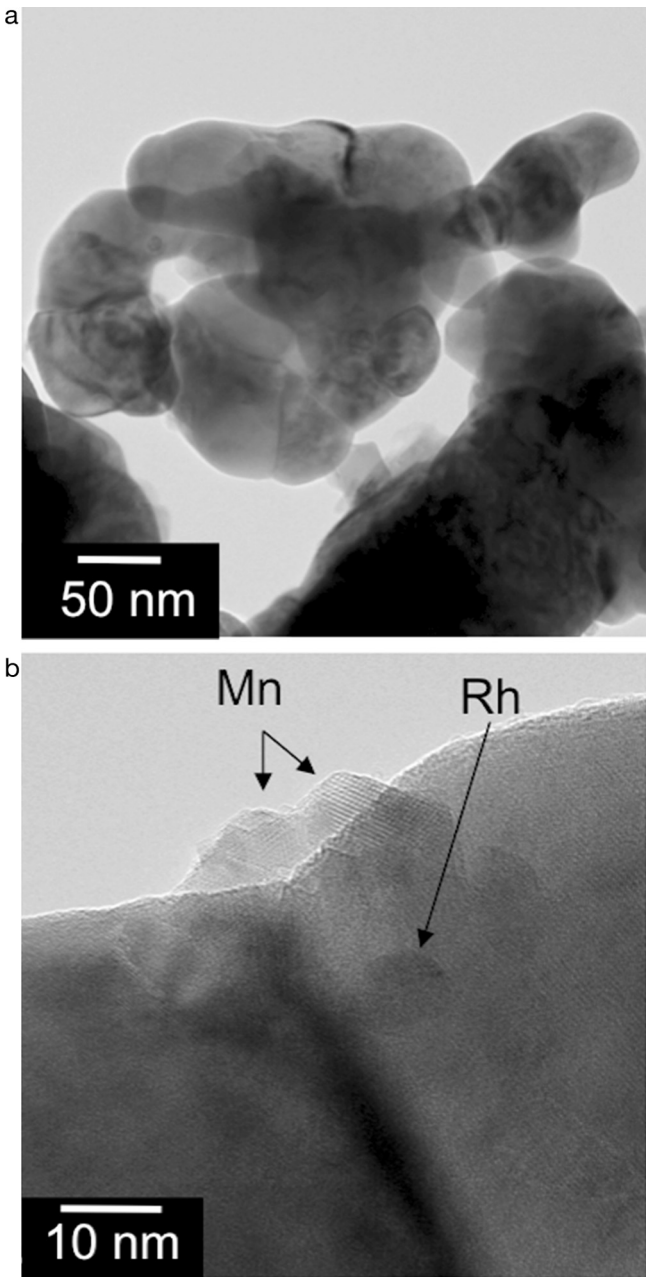

Fig. 5. TEM pictures of the Co-promoted sample a) Rh–Co alloy in the fresh material and b) Rh–Co alloy in the chemically aged material.

sample displays the lowest amount of coking with 40% less coke deposited compared to the Co-promoted sample. That the Co-promoted sample is the sample most prone to coke is not surprising since the combination of Rh and Co is known to coke [14,18]. Generally, a more acidic catalyst will be more prone to coke compared to a more basic catalyst [24]. The nature of the coke will also deviate between an acidic and a basic catalyst, where coke formed on an acidic catalyst will be more graphitic (lower H:C ratio), hence requiring higher temperatures to oxidize [25]. If the oxidation of coke is not catalyzed, the oxidation starts around 550 °C [26].

The La-promoted sample is the only material displaying distinct oxidation peaks at different temperatures: one low temperature peak starting at 250 °C and one merged high temperature peak, starting at 450 °C. The first peak is probably derived from coke deposited close to Rh particles, which catalyzes the oxidation and lowers the oxidation temperature [27,28]. The first high temperature peaks probably derive from coke deposited on the support. The temperature is too low to be uncatalyzed oxidation of coke

Table 3
The normalized amount of carbon deposited on the catalytic surface during the 7th cycle and after approximately 35 h on stream determined by temperature programmed oxidation (TPO). The numbers in parentheses denotes the nominal loading (wt.%) of the current metal.

Sample	Carbon deposited (a.u.)
Rh(1)Co(6)	2.3
Rh(1)La(6)	1.3
Rh(1)Mn(6)	1.8

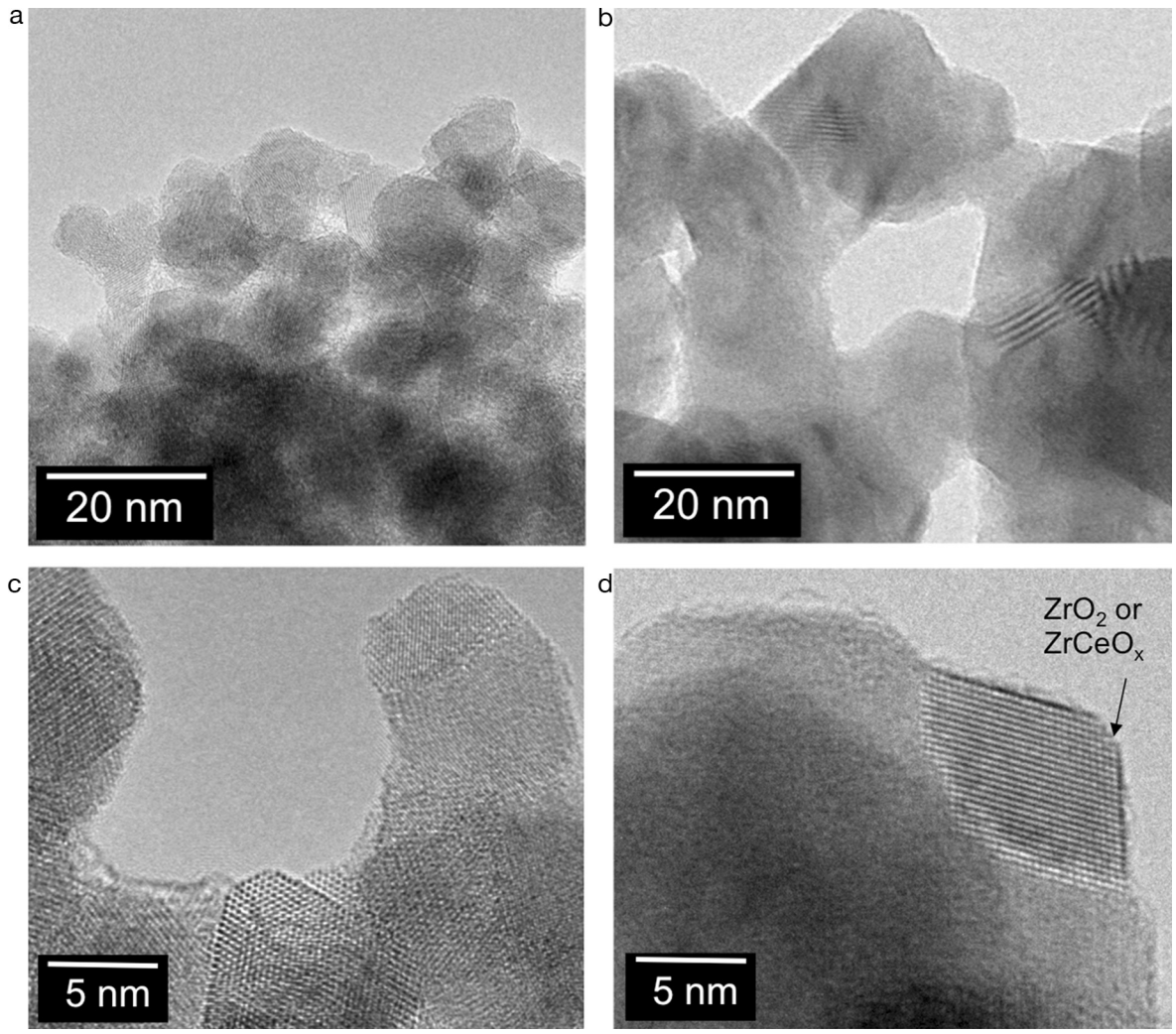

Fig. 6. TEM pictures of the La-promoted sample ((a and c) fresh sample, (b and d) aged sample).

[29]. However, it is not unlikely that ceria is catalyzing the coke oxidation [29]. The peak above 800 °C can either be highly graphitic coke being oxidized or decomposition of lanthanum dioxycarbonate ($La_2O_2CO_3$) to La_2O_3 and CO_2 [30]. $La_2O_2CO_3$ is easily formed when La_2O_3 is exposed to H_2O and CO_2 at elevated temperatures. The theory about the formation of carbonate is supported by the absence of a peak above 800 °C for the reference material (3 wt.% Rh) [31]. If this peak is due to decomposition of carbonate the amount of deposited coke is overestimated for the sample.

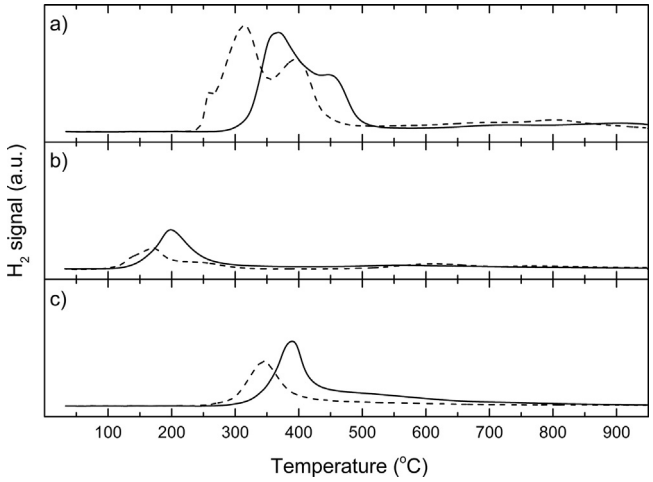

Fig. 7. TPR profiles for fresh and chemically aged catalyst samples, (a) Rh(1)Co(6), (b) Rh(1)La(6) and (c) Rh(1)Mn(6). The fresh samples are denoted with lines (——) and the chemically aged samples with dashed lines (- - -). The numbers in parentheses denotes the nominal loading (wt.%) of the current metal.

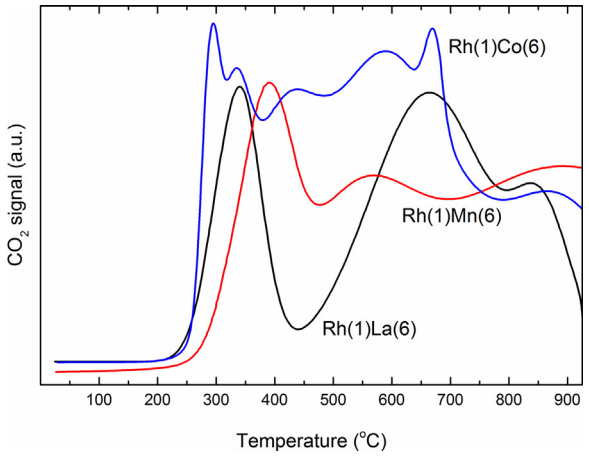

Fig. 8. The amount of coke deposited after the 7th experimental cycle (35 h on stream) measured with temperature programmed oxidation (TPO). The numbers in parentheses represent the nominal loading (wt.%) of the current metal.

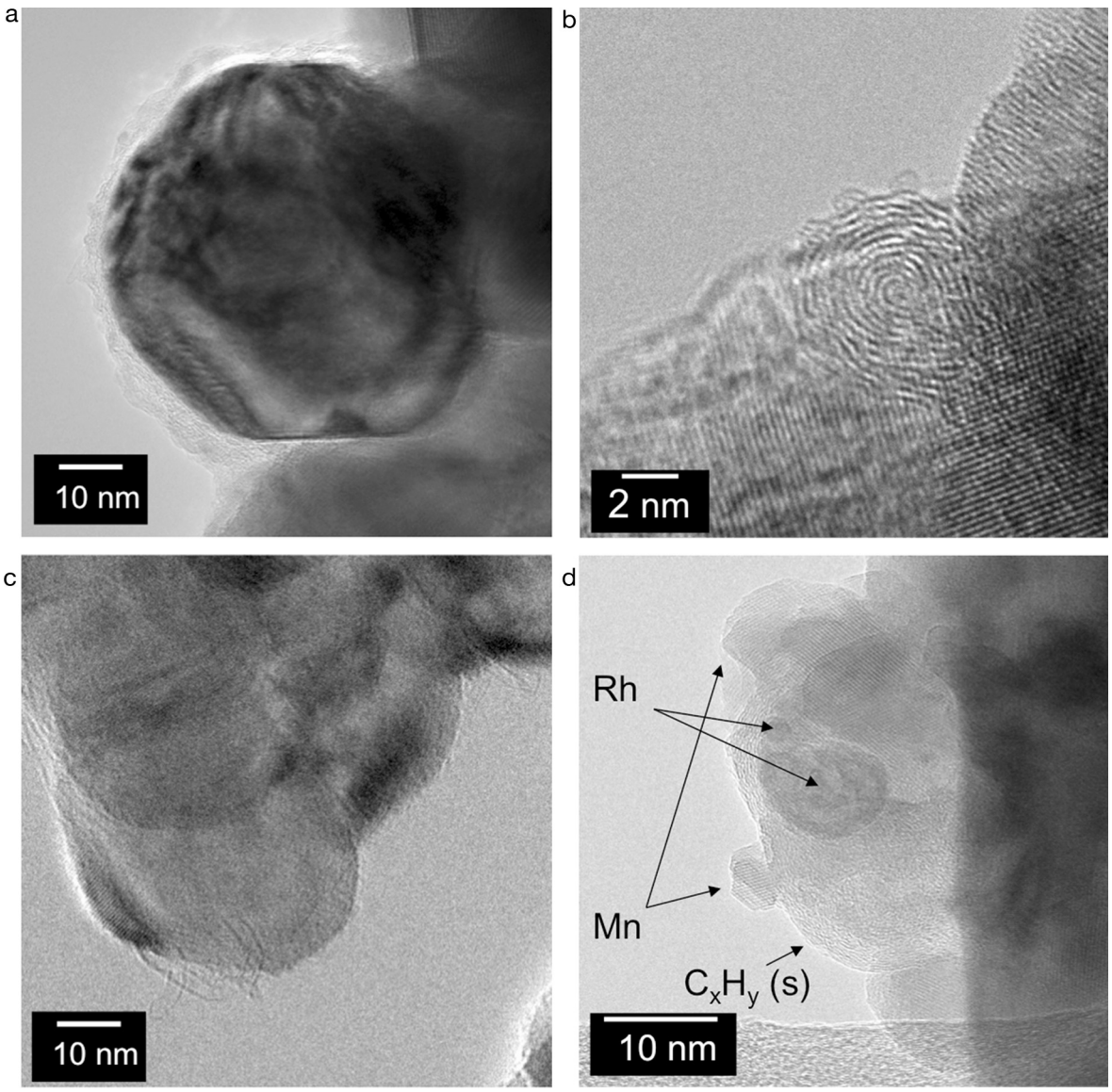

Fig. 9. Carbon residues on the samples observed with TEM after TPO analysis. (a) Encapsulating carbon layer in Co-promoted sample, (b) nanotubes in Co-promoted material, (c) soot particle on Mn-promoted material and (d) Mn and Rh particles embedded in coke in Mn-promoted material.

Additionally, promotion with La improves the material's resistance towards coking compared to the reference material [31]. The largest improvement is observed for coke deposited on the support of the catalyst, which is attributed to the presence of lanthanum.

In contrast to the La-promoted sample the other two samples reveal no clear peaks and high CO_2 signal throughout the entire temperature range. The highest CO_2 signal is observed for the Co-promoted sample where the peaks are closely merged together. The oxidation of coke starts at 250 °C with a sharp increase of the CO_2 signal followed by a second peak around 300 °C. These two peaks most likely belong to coke situated in the vicinity of an active site. The CO_2 signal continues to be high up to 700 °C where it drops to a lower level. The TEM analysis after TPO analysis of the Co-promoted sample revealed residues of coke (Fig. 9a and c). The residues consisted of several different types of coke; coke layers formed around the metal particles, residues of nanotubes and veils. The finding of nanotubes and layers around the metal particles is not surprising since Rh–Co catalyst has been reported previously to form both these types of coke [18,32]. Generally, nanotubes are said to grow with a metal particle on the top, causing the particle to be pushed out from the surface [33]. However, it was not possible to observe any metal particles at the end of the nanotubes by TEM, which might be that they have fallen back onto the support during the TPO analysis.

The Mn-promoted sample exhibits a clear low temperature oxidation peak at 400 °C followed by a constant high CO_2 signal. It can also be observed that the material has the highest initial temperature oxidation. The reason behind this is probably due to the presence of both coke free metal particles and metal particles encapsulated in large coke structures (Fig. 5b and Fig. 9d). The coke structure encapsulating the Mn and Rh particles is most probably graphene [33]. The first oxidation peak is believed to be originating from coke covering metal particles in thin layers and thereby the oxidation is catalyzed to a lesser extent compared to the other samples. The rest of the CO_2 signal is thought to be derived from coke layers burning off from the larger encapsulations. In addition, sphere shaped particles of highly ordered coke were observed in the material. These are believed to be multiple layers of graphene, which is a common structure found in soot [33].

Since coke residues were found in the Co and Mn-promoted materials after TPO analysis it is reasonable to believed that coke will build up on these materials even though regeneration is employed regularly. Despite the considerable amount of coke analyzed in the two materials, the initial activity is not affected to any wider extent. This is believed to be due to rhodium's high coke tolerance [17,27]. However, the build-up of coke is thought to the main reason behind the sharp deactivation after 20 h on stream of the Co-promoted material.

4. Conclusions

This is a follow-up study on a previous study (Ref. [11]) where three transition metals (Co, La, and Mn) were evaluated as promoters for 1 wt.% Rh supported on CeO_2–ZrO_2 catalyst for ATR fuel reforming. The aim was to investigate if it was possible to achieve the same catalytic activity as for a 3 wt.% Rh catalyst by promoting the 1 wt.% Rh catalyst. In this study, the focus is the changes in the material properties after time on stream.

The study shows that the three materials were aged in significantly different ways. However, all three materials showed a large decrease in surface area after thermal treatment in air. It is not unreasonable to assume that the thermal treatment is less damaging to the materials than the operating conditions. Therefore, it is likely that the surface area will decrease even more after time on stream, which was not possible to confirm with BET measurements due to the limited amount of aged material. However, the decrease of surface area is not reflected in the decrease of activity and therefore it is concluded that this is not one main characteristic influencing the activity of a fuel reforming catalyst. This corresponds well with that high-temperature reactions mainly take place on the outer surface of the material and not deep inside the pores.

The three promoters affect the material in different ways, lanthanum mainly affects the support, cobalt forms bimetallic particles with rhodium and manganese forms separate particles. The addition of lanthanum decreased the coke formation compared to the reference material (3 wt.% Rh/CeO_2–ZrO_2). The decrease was mainly observed for coke deposited on the support. Lanthanum also stabilized the CeO_2–ZrO_2 thereby preventing crystallite growth. In addition, it was observed to stabilize a dispersed Rh phase. The Co-promoted material displayed the highest activity of the evaluated materials. However, significant amount of coke was analyzed on the material after operation, which is believed to be the main reason for the deactivation observed after 25 h on stream. Addition of manganese initially sustained the formation of a dispersed Rh phase but the dispersion was not maintained during reaction and particle growth of both Rh and Mn was observed. As the Co-promoted material, this material also has a significant amount of coke deposited after operation.

The results show that by adding various transition metals the properties of the catalyst can be enhanced. If the advantages and disadvantages with the three materials are summarized, it can be concluded that the material promoted with lanthanum seems to have the highest potential. Even though the material does not show a stable activity in terms of H_2 yield after 35 h of operation the decrease is very slow. Additionally, enhancement in two important material characteristics are observed compared to the reference material: (i) the tendency for coking is decreased and the coke formed can be oxidized completely by elevated temperatures and oxidizing atmosphere, and (ii) the material has improved thermal stability which decreases the sintering of both rhodium and support.

Acknowledgments

The Swedish Foundation for Strategic Environmental Research (Mistra) together with KIC InnoEnergy through the project SynCon are gratefully acknowledged for their financial support. Knut and Alice Wallenberg Foundation is also acknowledged for their financial support to the EM equipment at MMK, Stockholm University.

Thanks to MEL Chemicals for providing the CeO_2–ZrO_2 support and Corning Inc., for supplying the cordierite monoliths. Thanks also to the Institute for Micro Process Engineering at Karlsruhe Institute of Technology (KIT) for valuable help with the diesel evaporator at KTH [34].

References

[1] United States Environmental Protection Agency (EPA), http://www.epa.gov/, (last visited: 26.05.14).
[2] M. Contestabile, Energy Policy 38 (2010) 5320–5334.
[3] S.M.A. Rahman, H.H. Masjuki, M.A. Kalam, M.J. Abedin, A. Sanjid, H. Sajjad, Energy Convers. Manage. 74 (2013) 171–182.
[4] F. Gunnarsson, M.Z. Granlund, M. Englund, J. Dawody, L.J. Pettersson, H. Härelind, Appl. Catal. B 162 (2015) 583–592.
[5] D.-J. Liu, T.D. Kaun, H.-K. Liao, S. Ahmed, Int. J. Hydrogen Energy 29 (2004) 1035–1046.
[6] Diesel Net http://www.dieselnet.com, (last visited: 15.04.14).
[7] P. Agnolucci, W. McDowall, Technol. Forcast. Soc. 74 (2007) 1394–1410.
[8] F. Baratto, U.M. Diwekar, J. Power Sources 139 (2005) 188–196.
[9] S. Specchia, V. Specchia, Ind. Eng. Chem. Res. 49 (2010) 6803–6809.
[10] A. Shamsi, J.P. Baltrus, J.J. Spivey, Appl. Catal. A 293 (2005) 145–152.
[11] M.Z. Granlund, K. Jansson, M. Nilsson, J. Dawody, L.J. Pettersson, Appl. Catal. B 154–155 (2014) 386–394.
[12] S. Naito, H. Tanaka, S. Kado, T. Miyao, S. Naito, K. Okumura, K. Kunimori, K. Tomishige, J. Catal. 259 (2008) 138–146.
[13] M. Araque, J.C. Vargas, Y. Zimmermann, A.-C. Roger, Int. J. Hydrogen Energy 36 (2011) 1491–1502.
[14] Y.-G. Jung, D.H. Lee, Y. Kim, J.H. Lee, S.-W. Nam, D.-K. Choi, C.W. Yoon, Bull. Kor. Chem. Soc. 35 (2014) 231–235.
[15] M. Ferrandon, T. Krause, Appl. Catal. A 311 (2006) 135–145.
[16] V. Perrichon, A. Laachir, S. Abouarnadasse, O. Touret, G. Blanchard, Appl. Catal. A 129 (1995) 69–82.
[17] R.K. Kaila, A. Gutiérrez, R. Slioor, M. Kemell, M. Leskelä, A.O.I. Krause, Appl. Catal. B 84 (2008) 223–232.
[18] T. Martínez, J.C. Vargas, A.C. Roger, Appl. Catal. B 132–133 (2013) 499–510.
[19] H.F.J. van't Blik, R. Prins, J. Catal. 97 (1986) 188–199.
[20] J.-R. Kim, W.-J. Myeong, S.-K. Ihm, J. Catal. 263 (2009) 123–133.
[21] W.Y. Hernández, O.H. Laguna, M.A. Centeno, J.A. Odriozola, J. Solid State Chem. 184 (2011) 3014–3020.
[22] L. Cao, L. Pan, C. Ni, Z. Yuan, S. Wang, Fuel Process. Technol. 91 (2010) 306–312.
[23] C. Diagne, H. Idriss, A. Kiennemann, Catal. Commun. 3 (2002) 565–571.
[24] M. Guisnet, P. Magnoux, Appl. Catal. A 212 (2001) 83–96.
[25] C.H. Bartholomew, R.J. Farrauto, Fundamentals of Industrial Catalytic Processes, 2nd ed., Wiley, Hoboken, N.J, 2006.
[26] C.E. Li, T.C. Brown, Energy Fuels 13 (1999) 888–894.
[27] E.I. Kauppi, R.K. Kaila, J.A. Lennekoski, A.O.I. Krause, M.K. Veringa Niemelä, Int. J. Hydrogen Energy 35 (2010) 7759–7767.
[28] S. Srihiranpullop, P. Praserthdam, Catal. Today 93–95 (2004) 723–727.
[29] I. Atribak, A. Bueno-López, A. García-García, J. Catal. 259 (2008) 123–132.
[30] B. Bakiz, F. Guinneton, M. Arab, A. Benlhachemi, J.-R. Gavarria, M. J. Condens. Matter 12 (2010) 60–67.
[31] M.Z. Granlund, S. Zacherl, L.J. Pettersson, Topics Catal. (2015) (in press).
[32] J.R. Rostrup-Nielsen, J. Catal. 27 (1972) 343–356.
[33] S. Helveg, J. Sehested, J.R. Rostrup-Nielsen, Catal. Today 178 (2011) 42–46.
[34] Institute for Micro Process Engineering, Karlsruhe Institute of Technology, http://www.imvt.kit.edu, (last visited: 10.10.14).